J. Fluid Mech. (1994), *vol.* 258, *pp.* 245–254

The dynamics of vorticity tubes in homogeneous turbulence

By A. VINCENT[1] AND M. MENEGUZZI[2]

[1]CERCA, 5160 bd Decarie, Montréal, Québec H3X 2H9, Canada *and* Département de Physique, Université de Montréal, Québec, Canada H3C 3J7

[2]CERFACS, 42 avenue Gustave Coriolis, 31057 Toulouse, France

(Received 18 June 1992 and in revised form 4 May 1993)

Analysis of data from a direct simulation of statistically steady homogeneous turbulence suggests that the vorticity tubes, which constitute the main structure of the vorticity field, are produced by shear instabilities. This is confirmed by a decay calculation, in which vorticity sheets appear at first, and then roll up to form the first tubes. These instabilities seem to be at least as important as vortex stretching in transferring energy from large to small scales.

1. Introduction

In a previous paper (Vincent & Meneguzzi 1991, called Paper I in the following), we presented some results of a direct simulation of statistically steady homogeneous turbulence computed on a 240^3 grid, with periodic boundary conditions, and deterministic forcing on a few large-scale modes. The Reynolds number R_L based on the integral scale L and the r.m.s. velocity v_0 was ≈ 1000, while R_λ, based on the Taylor microscale λ and v_0, was ≈ 150. The integration lasted more than 60 eddy turnover times (this time is defined as L/v_0). Refer to Paper I for definitions and details.

Our calculation confirmed the previous result by Siggia (1981) and others (Kerr 1985; She, Jackson & Orszag 1990) that the flow is organized in very elongated vorticity tubes. In addition, given our larger Reynolds number, we could show that these tubes are not limited to the dissipation-scale domain, but that they involve the inertial range scales as well, up to the integral scale L.

Paper I was concerned with the description of these structures and with the statistical properties of the flow, but did not attempt to answer questions about their dynamics: how they are produced in the first place, how they evolve and interact with each other, what is their typical lifetime, and how they are finally dissipated. Another question not dealt with is the importance of vorticity stretching, and the way these tubes reach such lengths. One would also like to know the role of these structures in the energy cascade through which kinetic energy is, on average, transferred from large to small scales. In the present work, we try to shed some light on these questions.

For this purpose, we have reanalysed the results of the calculation of Paper I, with particular attention paid to the time evolution of the vorticity structures of the flow. These results constitute an important data base, with a total of 260 complete stored velocity fields, representing 60 large-eddy turnover times of a statistically steady space-periodic turbulent flow (see Paper I for definitions). Let us call this calculation 'Run A'. In addition, in order to isolate the mechanism of vorticity tube generation, we have performed a decay calculation, at a resolution of 256^3, with a random initial condition involving large scales only, which we call 'Run B'. We first discuss the mechanism of

vorticity tube generation, then the vortex stretching and the role of these tubes in the inertial-range casade.

2. The mechanism of vorticity tube generation

To visualize the vorticity field in three dimensions, we plot a perspective view of the field represented by arrows on a three-dimensional grid, as was done in Paper I. Only vectors with modulus above a certain threshold are plotted. Control of this threshold helps the observer to follow a given structure. In Paper I, it was conjectured that the vorticity tubes observed are generated by shear instabilities. When running a film obtained with this type of visualization, this is immediately suggested by the fact that the tubes often appear in pairs or in groups of several that are approximately parallel, moving in the same plane, in a direction perpendicular to their axis. One also observes a succession of tube formations with approximately the same alignment and in the same area of the fluid. An example of this is given by figure 1. Figure 1 (*b*) displays the same view of the vorticity field as figure 1 (*a*) a little more than one turnover time later. The tubes marked A, B, C, D are seen to move in a direction perpendicular to their axis, while D and E are merging.

The tubes appear with a finite length above our threshold. During their lifetime, they are often clearly seen to increase in length, by a factor two or three. This implies that the shear instabilities occur in a zone of the fluid submitted to strong stretching.

A precise definition of the typical tube lifetime is difficult owing to the need to use an amplitude threshold. In figure 1, the threshold vorticity amplitude is 55, while the maximum vorticity is 223. (Our units are such that the periodic box size is 2π, the r.m.s. velocity is ≈ 1, and the turnover time is also ≈ 1.) If this threshold is held fixed in time, the tubes appear with a finite length and can be followed for several turnover times (typically 5), and then disappear. The true lifetime of the structures is probably twice as large. The tubes are therefore 'coherent structures' in the sense that they definitely last longer than one turnover time.

In order to investigate the mechanism of production of vorticity, we explore in more detail a sphere extracted from the basic 240^3 cube of run A, 80 grid points in diameter, centred near tubes A, B, C, D of figure 1. Figure 2 (*a*, *b*) shows the vorticity field in this subdomain at two different times, close to those of figure 1. The large tube at the centre of figure 2 (*b*) is seen to be the result of the merging of previously parallel tubes which seem to originate from the same shear zone. This is shown more clearly in figure 3, which displays a different view of the flow detail of figure 2 (*a*), a view approximately along the axis of the parallel tubes. One can see the velocity in a plane perpendicular to the tubes.

This vortex merging leading to a stronger vorticity structure is generally the origin of the largest tubes observed. Some of them have undergone several mappings. The phenomenon seems much less important for the large number of medium size of tubes.

In order to better isolate the mechanism of tube formation, we have performed the decay run B, at resolution 256^3. Like in Paper I, we solve the Navier–Stokes equation with periodic boundary conditions by a Fourier pseudo-spectral method, but with no forcing term. The initial condition is a random field with only a few small-wavenumber components. Initially, the vorticity is very small. When one watches the evolution of the vorticity field above a fixed threshold, the first velocity structures which appear are pancake-like zones, which flatten with time. The same structures are seen in solutions of the Euler equation (Brachet *et al.* 1992; Pumir & Siggia 1991; R. Kerr and J. R. Herring 1992, private communication). The flattening leads to the appearance of

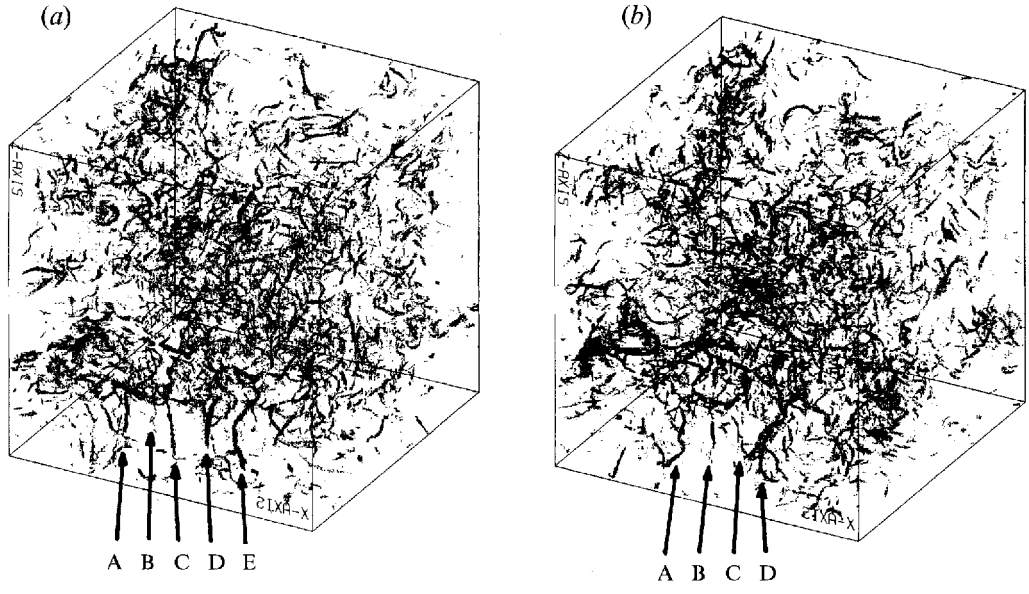

FIGURE 1. (*a*) View of the vorticity field: vorticity vectors are represented by arrows, here too small to be seen individually. Only vectors with modulus above a certain threshold are displayed. The tubes marked A, B, C, D, E are approximately parallel. (*b*) The same as (*a*) a little more than one turnover time later. Note the parallel motion of tubes A, B, C, D and the merging of the tubes D and E.

sheets, which tend to bend and roll up, producing the first vorticity tubes. During this process, the vorticity is observed to increase. Therefore, the shear instability is accompanied by vortex stretching. An example of this process is shown in figure 4(*a*, *b*) (plate 1). The colour scale is kept constant in time, dark blue indicating larger vorticity vectors than light blue, and red even larger. The tips of the vectors' are shown by white dots. The same conclusion was reached by Brachet *et al.* (1983) in their study of the solution of the Navier–Stokes equations with a Taylor–Green vortex as initial condition. A self-similar model of the flattening of the vorticity zones leading to sheets is presented in Brachet *et al.* (1992). Vorticity sheets rolling-up to form tubes are also seen in the statistically steady-state run (run A), but they are smaller and subjected to strong perturbation from the surrounding vortices.

A model of turbulence by Lundgren (1982) involves spiral structures around vorticity tubes, generated by merging of several tubes. In what we see, there is in some cases a spiral structure due to the rolling up of a vorticity sheet, but this a transient phase, after this structure seems to be forgotten. Indeed, we have examined (Paper I) the structure of many such tubes and the vorticity profile across them does not display a series of spikes, as expected if they were rolled-up sheets. Further evidence supporting this conclusion is provided by the distribution of dissipation rate in space. Figure 5 (plate 2) shows the large vorticities in green and large dissipation rates in red. One can see that the dissipation occurs in the vicinity of but outside the vorticity tube cores. If these cores had a spiral structure, the corresponding strong shear layers would show up in pictures of the dissipation rate. After the roll-up phase leading to a vorticity tube, the viscosity probably destroys the spiral structure and the resulting vortex core has an approximate solid-body rotation. The spiral structure proposed by Lundgren therefore exists in some cases but during a time much shorter than the typical vorticity tube lifetime. Our conclusion about the dissipation being around the vorticity tubes has already been reached by Kerr (1985) and Brachet (1991).

(*a*)

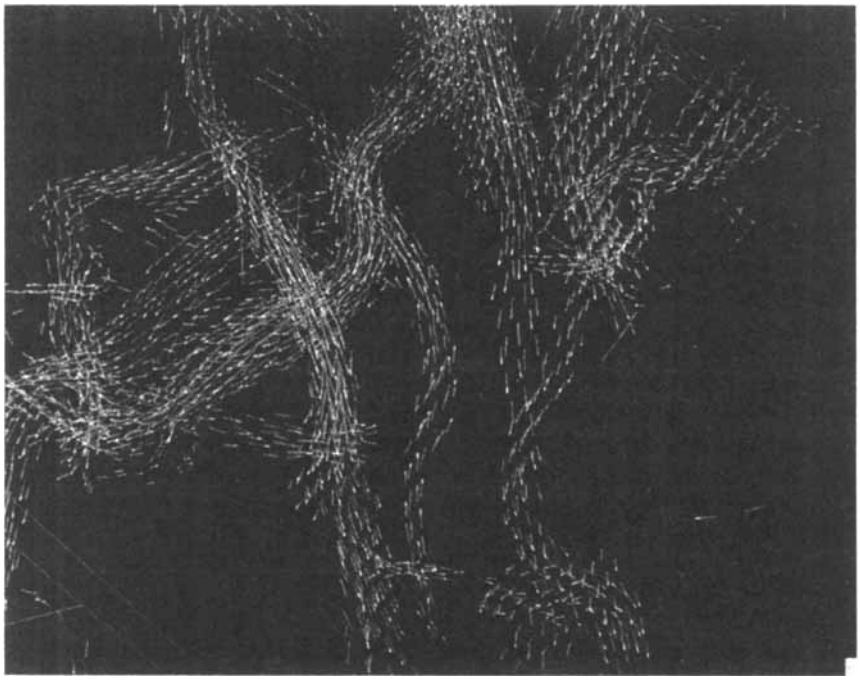

(*b*)

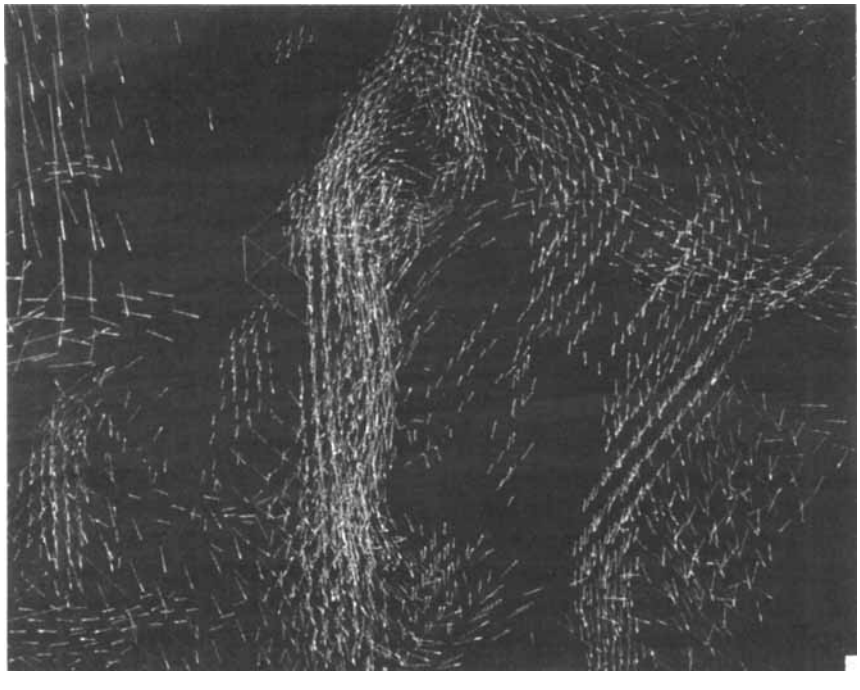

FIGURE 2. (*a*) Detail of the vorticity field showing two approximately parallel tubes; with a secondary counter-rotating tube between them. (*b*) The same vorticity region as (*a*) one turnover time later. The three vorticity tubes of (*a*) have merged into one larger tube.

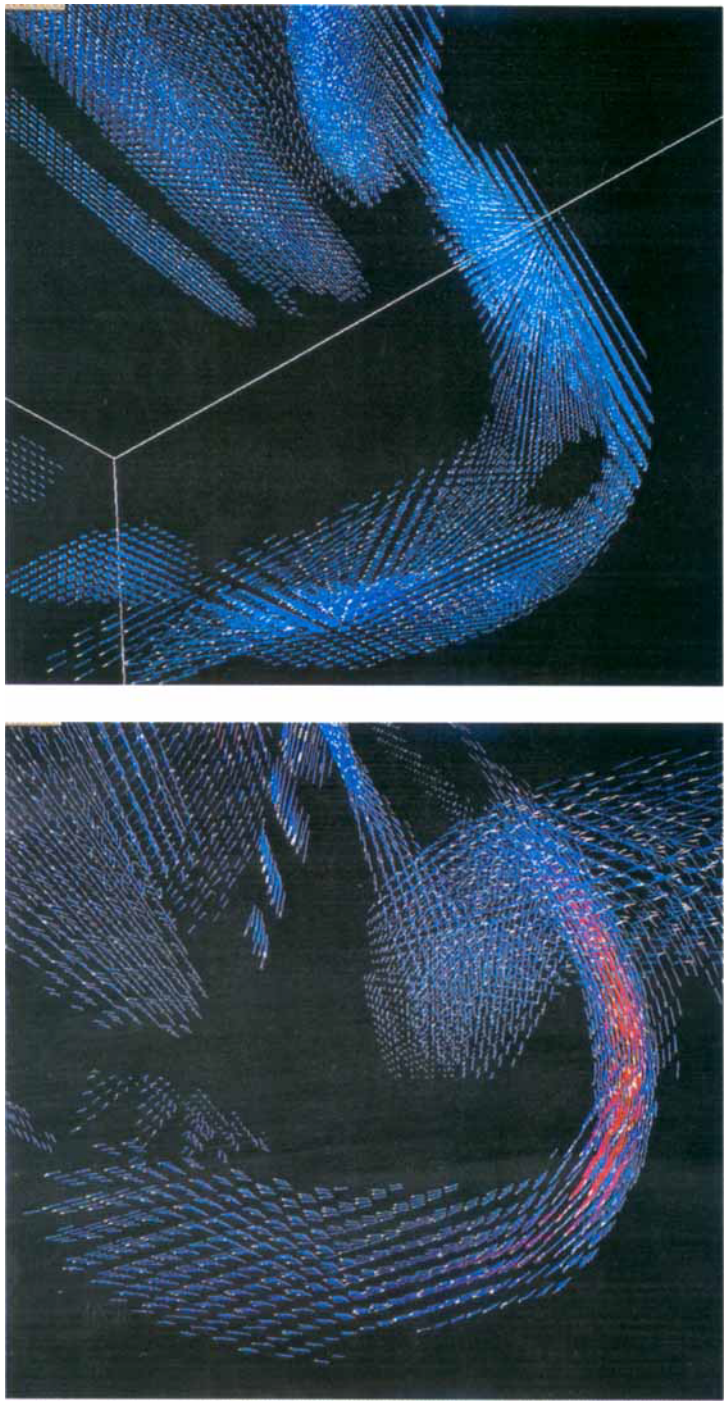

FIGURE 4. *(a)* Detail of the vorticity field of run B, at early times, showing several curved vorticity sheets. Dark blue indicates larger vorticity than light blue, and red even larger. *(b)* Same as *(a)* a few turnover times later. The first tubes have appeared, as a result of the rolling-up of some of the vorticity sheets, and the vorticity has increased.

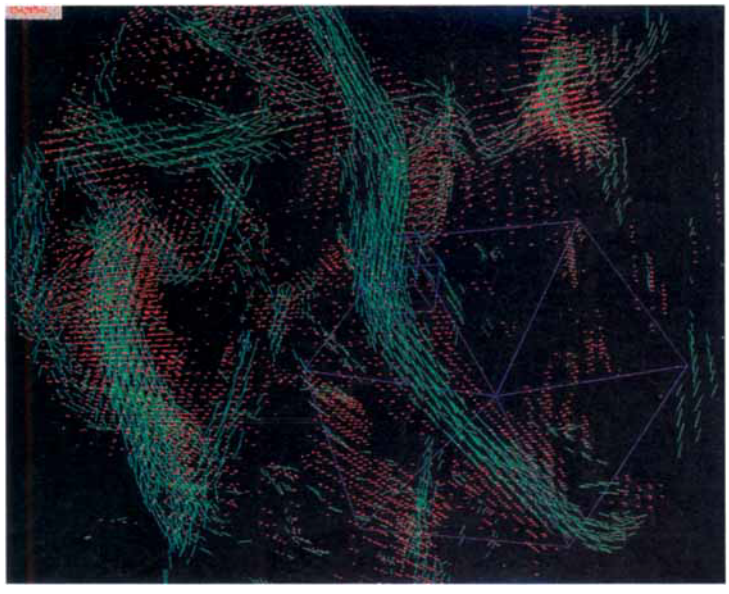

FIGURE 5. Detail of the vorticity field of run A, in green, with the regions of large dissipation shown in red.

FIGURE 8. Detail of the velocity field after filtering in Fourier space so as to retain a fraction of the inertial domain. In red: low-wavenumber range of the inertial domain; in green: intermediate range; in yellow: high-wavenumber range.

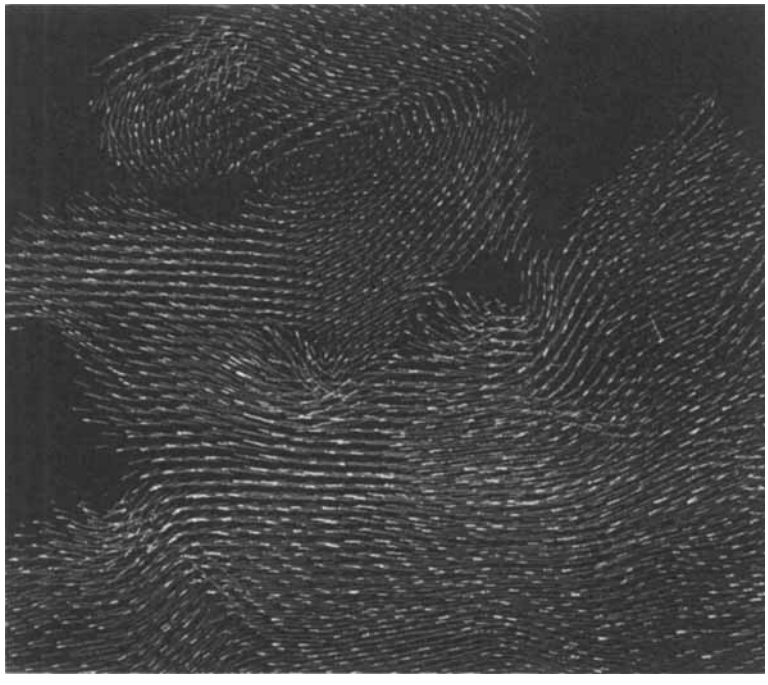

FIGURE 3. The velocity field in a plane approximately perpendicular to the vorticity tubes.

We have computed the eigenvectors and eigenvalues of the strain tensor around these unstable vorticity sheets. As in paper I, λ_1, λ_2 and λ_3 are the eigenvalues of the rate-of-strain tensor $S_{ij} = \frac{1}{2}(\partial_i v_j + \partial_j v_i)$, in ascending order, with λ_1 always negative and λ_3 always positive, and $\boldsymbol{e}_1, \boldsymbol{e}_2, \boldsymbol{e}_3$ the eigenvectors associated with $\lambda_1, \lambda_2, \lambda_3$ respectively. ($\boldsymbol{\nabla} \cdot \boldsymbol{v} = 0$ implies $\lambda_1 + \lambda_2 + \lambda_3 = 0$). In pure shear, for instance $v_x = y$, $v_y = v_z = 0$, one would have $\boldsymbol{e}_1$ and $\boldsymbol{e}_3$ at 45° in the (x, y)-plane, i.e. $\boldsymbol{e}_1 = (1, -1, 0)$, $\boldsymbol{e}_3 = (1, 1, 0)$, and $\boldsymbol{e}_2 = (0, 0, 1)$. If a straining field is present, for instance $v_x = ax + y$, $v_y = -ay$, $v_z = 0$, for large values of a, $\boldsymbol{e}_3$ will be close to the x-axis, and $\boldsymbol{e}_1$ close to the y-axis.

What we observe in run B is the following. At early times, $\boldsymbol{e}_1$ is oriented perpendicularly to the vorticity pancakes, while the vorticity is parallel to the pancakes and sometimes to $\boldsymbol{e}_3$. At a fraction of a turnover time later, $\boldsymbol{e}_1$ is still perpendicular to the pancake, but the vorticity has become aligned with the intermediate eigenvector $\boldsymbol{e}_2$. At roughly two turnover times, the pancake has become a thin vorticity sheet, which is beginning to bend, and the vorticity is still aligned with $\boldsymbol{e}_2$. But we observe that $\boldsymbol{e}_1$ and $\boldsymbol{e}_3$ are now approximately at 45° respect to the plane of the sheet. So the picture is that of an initial straining phase which produces a vorticity sheet, with the shear increasing and becoming dominant in a second phase, followed by the rolling up of the sheet. This scenario was in fact suggested some time ago by Betchov (1976).

In this rolling-up phase leading to tube formation, $\boldsymbol{\omega}$ is already aligned with the intermediate eigenvector $\boldsymbol{e}_2$. Therefore, the general alignment of the intermediate strain eigenvector with $\boldsymbol{e}_2$ found previously by Kerr (1985) and ourselves in Paper I happens long before the vorticity tube production.

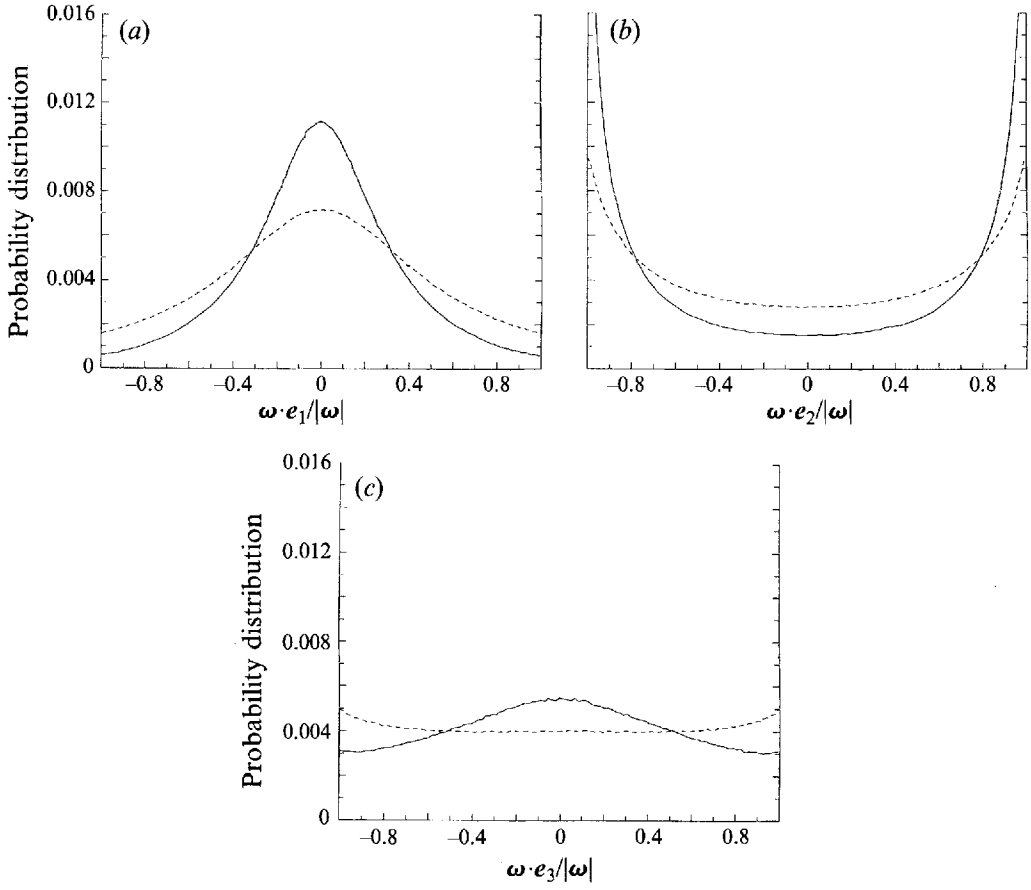

FIGURE 6. Distribution of the angle between the vorticity field and the rate of strain eigenvectors. Continuous line: large vorticities; dashed line: small vorticities. (*a*) Eigenvector $\boldsymbol{e}_1$ associated with the smallest eigenvalue λ_1 (always negative); (*b*) eigenvector $\boldsymbol{e}_2$, associated with the intermediate eigenvalue λ_2; (*c*) eigenvector $\boldsymbol{e}_3$, associated to the largest eigenvalue λ_3 (always positive).

3. Vortex stretching

As already mentioned, the vorticity tubes appear with a finite length, and their length is subsequently increased by stretching due to velocity gradients. Observing many tubes, we find that their length increases by a factor 2 or 3 during their lifetime. It is known that a line element is stretched on average by homogeneous isotropic turbulence (Cocke 1969; Orszag 1970, 1977). This is probably connected with the fact that the intermediate strain eigenvalue λ_2, which corresponds to the eigenvector generally parallel to the vorticity, is more often positive than negative. However, it seems that the most intense tubes result from instabilities of vorticity sheets produced by a strong strain, a more systematic effect.

A quantitative measure of this alignment of vorticity with λ_2 was presented in Paper I by plotting the distribution of the cosine of the angles between the vorticity $\boldsymbol{\omega}$ and the strain eigenvectors $\boldsymbol{e}_i$. These distribution functions are very similar to the ones found in experiments by Tsinober, Kit & Dracos (1992), and numerically by Ashurst *et al.* (1987). It was not clear why the distribution of $\boldsymbol{\omega}\cdot\boldsymbol{e}_3/|\boldsymbol{\omega}||\boldsymbol{e}_3|$ is so much flatter than the others. In order to clarify this point, we have recomputed these distributions after splitting the set of vorticity values into large and small vorticities, i.e. $\omega > \omega_0$ and

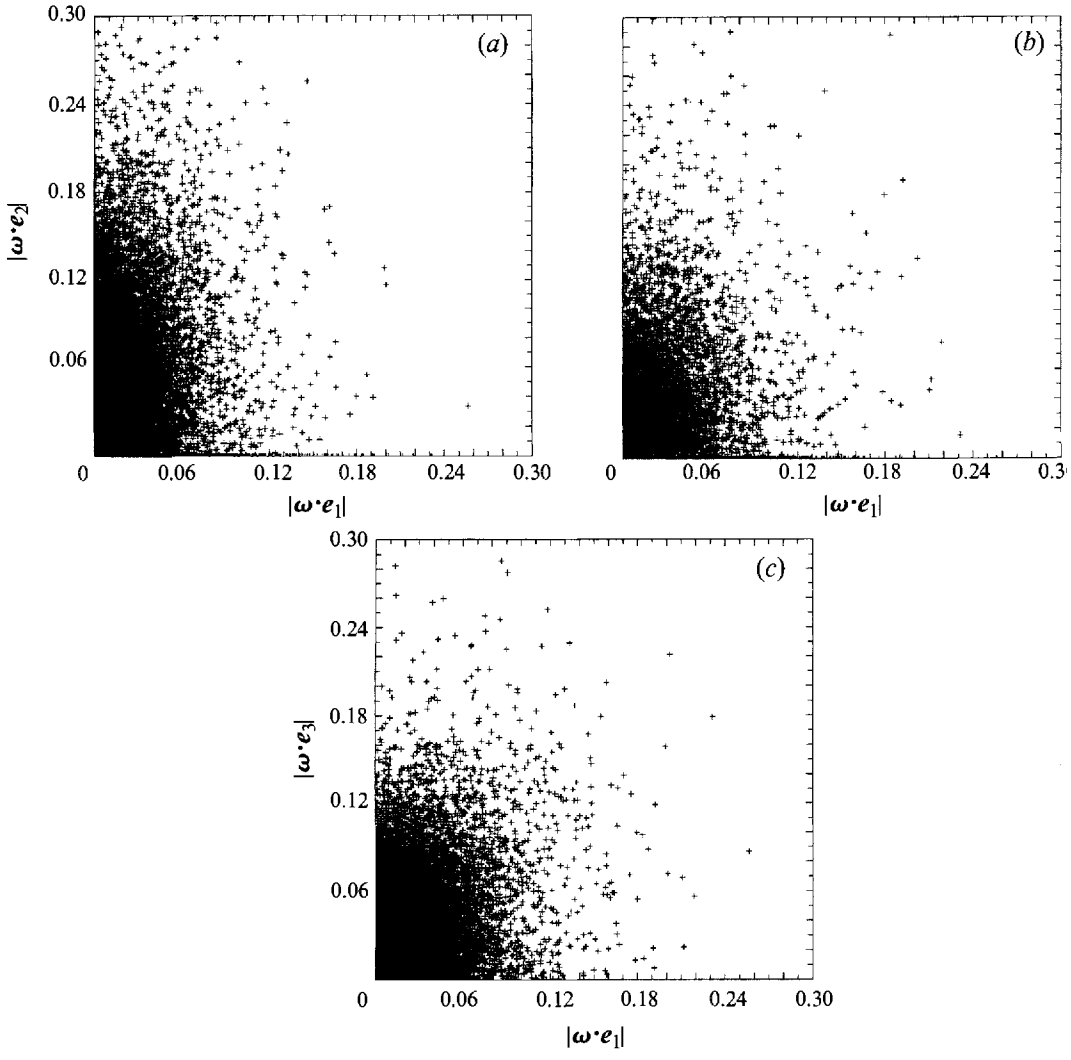

FIGURE 7. Tip of the vorticity vector in the reference frame (e_1, e_2, e_3). (*a*) Projection on the plane (e_1, e_2) for $\lambda_2 > 0$. (*b*) Same as (*a*) but for $\lambda_2 < 0$. (*c*) Projection on the plane (e_1, e_3).

$\omega < \omega_0$. The value of ω_0 is 13 while the maximum ω value is 223. The volume in space occupied by the first set is 36%. The distributions are shown on figure 6(*a–c*). The alignment of ω with e_2 is more pronounced in large-vorticity regions than in the plot for the general field (see Paper I). For small vorticities, the distribution is flat, and there are definitely regions where ω and e_3 are parallel. In order to understand why the distribution of $\omega \cdot e_3/|\omega||e_3|$ is so much flatter than the other two, we have plotted (figure 7) the tip of the vorticity vector ω in the reference frame (e_1, e_2, e_3). The preferential alignment of ω with e_2 is clearly visible, as is the fact that λ_2 is more often positive than negative. Figure 7(*c*) shows that ω is more aligned with e_3 than with e_1 for small ω, but that there is little preferential alignment with one or the other for large ω.

Physically, we interpret this as meaning that although the vorticity, in large-vorticity regions, is more often aligned with the intermediate eigenvector e_2, random stretching nevertheless produces some vorticity along the main positive stress direction e_3. The

Time	η_1	η_2	η_3
5.92	−285	344	557
14.92	−404	438	775

TABLE 1

fact that large- and small-vorticity regions have different alignment produces a flat distribution when both are included in the statistics. In decay calculations, where the random stretching effect does not have enough time to become important, the alignment of $\boldsymbol{\omega}$ with $\boldsymbol{e}_2$ is much clearer, as shown in Brachet *et al.* (1992).

To make this more quantitative, we have computed, like Tsinober *et al.* (1992), the rate of enstrophy production $\eta = S_{ij}\omega_i\omega_j$. But in addition we have also computed separately the contributions of the three principal strain directions. The production rate in direction $\boldsymbol{e}_i$ is given by

$$\eta_i = \lambda_i(\boldsymbol{\omega}\cdot\boldsymbol{e}_i)^2,$$

with $\eta_1+\eta_2+\eta_3 = \eta$, the eigenvectors $\boldsymbol{e}_i$ having modulus 1. Table 1 gives the values of η_i at two different times. One can see that the enstrophy is produced in approximately equal amounts in directions 2 and 3, despite the fact that the stretching is much larger along direction 3.

A scenario was proposed by Ashurst *et al.* (1987) in which vorticity tubes are created at random by the mechanism of vorticity stretching, and then the induced stress tensor is such that the alignment of $\boldsymbol{\omega}$ with $\boldsymbol{e}_3$ shifts to an alignment with $\boldsymbol{e}_2$. If this picture were correct, one would expect η_3 to be dominant.

Our visualizations suggest another possibility. If the main mechanism of vorticity tube production is shear instability of strained vorticity sheets, the stress tensor is, when this instability develops, such that $\boldsymbol{\omega}$ is oriented in the $\boldsymbol{e}_2$ direction. In this case, η_3 is not expected to be much larger than η_2, which is what we observe.

4. The role of vorticity tube formation in the energy cascade

It was shown in Paper I that, after filtering the vorticity field in Fourier space so as to retain only the inertial-range scale, the field in physical space still appears organized in vortex tubes. When we look at the time evolution of the velocity and vorticity fields of run A after this kind of filtering, we observe essentially the evolution of the external part of the vorticity tubes.

To analyse the inertial range velocity field in more detail, we have taken several Gaussian filters in Fourier space, separating the inertial domain in three zones, and we have transformed the three fields back to physical space. Figure 8 (plate 2) shows a cut of the velocity field of run A. The low-wavenumber part of the inertial domain ($k \approx 10$) is shown in red, the intermediate part ($k \approx 15$) in green, and the higher wavenumber part ($k \approx 20$) in yellow. The figure suggest that the rolling-up of vorticity sheets plays an essential role in the energy cascade from large to small scales.

This picture is somewhat at variance with the traditional view of a Richardson many-step cascade, in which large eddies produce smaller eddies, smaller eddies produce even smaller ones, and so on. On the contrary, what we observe here – the production of vorticity sheets and their rolling-up to form vorticity tubes – is a one-step process, with a strong correlation between small and large scales. The small-scale vorticity constitutes the core of the vorticity structures seen in pictures of the inertial

domain. The resulting field is much more intermittent than what would be obtained in a many-step process. But an inertial range is definitely present in the energy spectrum, with an approximately $k^{-\frac{5}{3}}$ slope, as shown in Paper I.

One could object that our Reynolds number is not very large (1000) and that the Richardson cascade picture is envisaged in the limit of infinite Reynolds number. This may be true, but an experiment at $R = 80000$ (Douady, Coudet & Brachet 1991) also shows the appearance of very long vorticity tubes generated by a shear zone, very similar to our smaller-R results, and which are also suggestive of a one-step process.

Of course, one expects the formation of secondary vortices induced by the strong shear around the large tubes observed. Secondary vorticity tubes are indeed observed, approximately antiparallel to the primary one. An example is seen in figure 2(*a*).

The tube mergings we observe also contribute to the energy cascade to small scales. They probably also involve some energy backscatter from small to large scales, since the final product is a larger structure.

5. Conclusions

Our visualizations strongly suggest shear instabilities of thin vorticity sheets as the mechanism of vortex tube generation in three-dimensional turbulent flow. The general picture is that encounters between different parts of the fluid will inevitably produce shear layers (Betchov 1976). These sheets are unstable to vorticity tube formation, in typically one turnover time. The tubes are more stable than the sheets, and are therefore the dominant structures seen in a picture of steady-state turbulent flow. The alignment of vorticity with the intermediate strain eigenvector is found to exist before the shear instability develops, and is the result of vorticity sheet production by strong strain. It is not a consequence of tube formation.

The enstrophy production rates in the principal strain tensor directions as well as the visualization of the inertial-range velocity field in several bandwidths suggest that both the vorticity sheet production phase and the succeeding shear instability play an essential role in the energy cascade from large to small scales. To make this conclusion more quantitative, and assess the relative importance of these mechanisms, a more detailed study of the energy transfer (locally in space) is necessary.

We thank P. L. Sulem for numerous discussions and suggestions. All our calculations were done on the Cray-2 of the CCVR (Centre de Calcul Vectoriel pour la Recherche), Ecole Polytechnique, Palaiseau, France, thanks to a grant by CNRS (Centre National de la Recherche Scientifique).

REFERENCES

ASHURST, W. T., KERSTEIN, A. R., KERR, R. M. & GIBSON, C. H. 1987 *Phys. Fluids* **30**, 2343.

BETCHOV, R. 1976 *Archi. Mech. Stosowanej* **28** (5–6), 837.

BRACHET, M. E. 1991 *Fluid Dyn. Res.* **8**, 1.

BRACHET, M. E., MEIRON, D. I., ORSZAG, S. A., NICKEL, B. G., MORF, R. H. & FRISCH, U. 1983 *J. Fluid Mech.* **130**, 411.

BRACHET, M. E., MENEGUZZI, M., VINCENT, A., POLITANO, H. & SULEM, P. L. 1992 *Phys. Fluids* A **4**, 2845.

COCKE, W. J. 1969 *Phys. Fluids* **12**, 2488.

DOUADY, S., COUDER, Y. & BRACHET, M. E. 1991 *Phys. Rev. Lett.* **67**, 983.

KERR, R. 1985 *J. Fluid Mech.* **153**, 31.

LUNDGREN, T. S. 1982 *Phys. Fluids* **25**, 2193.

ORSZAG, S. A. 1970 *Phys. Fluids* **13**, 220.

ORSZAG, S. A. 1977 In *Fluid Dynamics* (ed. R. Balian & J. L. Peube). Les Houches Summer School, 1973. Gordon and Breach.

PUMIR, A. & SIGGIA, E. D. 1992 *Phys. Fluids* A **4**, 1472.

SHE, Z. S., JACKSON, E. & ORSZAG, S. A. 1990 *Nature* **344**, 226.

SIGGIA, E. D. 1981 *J. Fluid Mech.* **107**, 375.

TSINOBER, A., KIT, E. & DRACOS, T. 1992 *J. Fluid Mech.* **242**, 169.

VINCENT, A. & MENEGUZZI, M. 1991 *J. Fluid Mech.* **225**, 1 (referred to herein as Paper I).